Optical and Quantum Electronics (2024) 56:1347
https://doi.org/10.1007/s11082-024-07240-7

Structural, optical and dielectric studies of KCl modified TeO_2–Bi_2O_3–B_2O_3 glasses

Komal Poria[1] · Rajesh Parmar[1] · Sunil Dhankhar[2] · R. S. Kundu[3]

Received: 21 May 2024 / Accepted: 1 July 2024 / Published online: 23 July 2024

Abstract

The quaternary glass system $60TeO_2$-$(25-x)Bi_2O_3$-$15B_2O_3$-xKCl has been prepared by the melt-quenching process with x ranging from 0 to 20 mol%. X-ray diffraction patterns confirmed the amorphous nature of the synthesized glasses, showing no sharp crystalline peaks. The techniques field emission scanning electron microscopy and energy dispersive X-ray spectroscopy provide information about the surface morphology and elemental composition of the synthesized glass system, respectively. Physical parameters such as density, molar volume, ion concentration, interionic distance, polaron radius, and cation field strength were calculated to determine structural stability. Density and molar volume both decrease with an increase in KCl content. Oxygen packing density decreases with increasing KCl concentration, indicating a rise in non-bridging oxygen atoms. Using differential scanning calorimetry, the glass transition temperature (T_g) was calculated. Its value is found to decrease as the KCl content increases. FTIR and Raman spectra indicate the transformation of TeO_4 units into TeO_3 units and BO_4 units into BO_3 units with an increase in KCl content. The diffuse reflectance spectra method is used to study optical parameters such as optical band gap, cut-off wavelength, Urbach energy, refractive index, and metallization criteria. The optical indirect band gap energies (E_{opt}) range from 2.78 to 3.31 eV and are calculated by applying Tauc's relation. On the other hand, the values of the urbach energy (E_U) vary from 0.289 to 0.183 eV, indicating disorderliness or defects in the glass samples decrease with increasing KCl content. The synthesized glasses can be considered for non-linear optical applications since their metallization criterion (M) values ranged from 0.373 to 0.407. The dielectric parameters of the glasses were calculated on a frequency scale of 10^{-1} to 10^6 Hz by varying the temperature from 453 to 553 K. Dielectric analysis of the as-prepared glasses shows the non-Debye type behavior.

Keywords Tellurite · EDX · FTIR · Raman · Metallization · Dielectric loss

✉ Rajesh Parmar
rparmar1996@gmail.com

[1] Department of Physics, Maharshi Dayanand University, Rohtak 124001, India

[2] Department of Physics, Govt. College for Women, Lakhan Majra, Rohtak 124001, India

[3] Department of Physics, Guru Jambheshwar University of Science and Technology, Hisar 125001, India

1 Introduction

Tellurite glasses are distinguished by their promising optical characteristics which include good transmission in the infrared region, superior thermal stability, chemical resistance, broad range of homogeneity, low melting point, high linear and non-linear refractive indices, and low melting temperatures (El-Mallawany and El-Mallawany 2001; Alshamari et al. 2023; Poria et al. 2024). These qualities make them useful for various applications including UV-induced photo-optical switches, refractive gratings, and optical fiber amplifiers (Kundu et al. 2014; Rammah et al. 2019). It is known that B_2O_3 is a glass former that forms glass very well, even at normal quenching rates. The structure of pure vitreous B_2O_3 is composed of a disordered pattern of boroxyl rings and BO_3 triangular units connected by B–O–B bonds (Al-Ghamdi et al. 2021). Low melting temperatures, excellent clarity, and resistance to devitrification are characteristics of boro-tellurite glass networks (Aloraini et al. 2021). The presence of BO_3, B_3O_6, and TeO_4 structural units that impact the distances between Te–O, Te–Te, O–O and B–O bonds were identified during the structural investigation of a binary B_2O_3–TeO_2 glass system (Saddeeka et al. 2018; Elkhoshkhany and El-Mallawany 2015). Bismuth oxide (Bi_2O_3) has attracted a lot of attention due to its applications in optical and optoelectronic devices, thermal and mechanical sensors, reflecting windows, and other domains (Kashif et al. 2018; Abdelghany et al. 2024; Gupta et al. 2017). These oxide glasses are appropriate for nonlinear optical applications because of the low field strength and strong polarizability of the Bi^{3+} ions. Because bismuth oxide has a low field strength of Bi^{3+} ions, it is rarely regarded as a network growing in isolation. However, over a comparatively wide composition range, glass production becomes viable when combined with B_2O_3 (Berwal et al. 2017, 2015).

Alkali ions, such as K, Na, and Li can be added to tellurite glass to lower its melting point, weaken its bonds, and reduce network connectivity. In contrast, tellurium oxide (TeO_2) the conditional glass-former, often does not transition into a glassy state alone as a pure oxide due to the specific mechanism by which tellurite glasses form Sidkey and Gaafar 2004; Lee et al. 2008. As a result, adding alkali ions to tellurite-based glasses increases their ability to form glass, resulting in the formation of (NBO) sites and lowering the average coordination number (Ersundu et al. 2017). When alkali ions are injected, they significantly improve the optical characteristics of glasses, particularly those containing heavy element oxides (Bahgat and Abou-Zeid 2001). Hussein et al. 2022 examined the impacts of incorporating alkali ions, such as KCl, and assessed their effects using an optical spectroscopic examination of the tellurite glass system. The optical spectra of the Eu^{3+} ion doped in $ZnCl_2$–$BaCl_2$–KCl glasses have been examined by Annapurna et al. 2002. Wang et al. 2013 synthesized a novel variety of tellurite glasses doped with Yb^{3+} and composed of TeO_2, K_2O, ZnO, and Al_2O_3 displaying exceptional thermal stability and a high emission cross-section.

The present study's novelty emphasizes the importance of this glass composition in a wide range of technical applications, such as optical fibers, design laser devices, IR technologies, thermal image guides, optoelectronics, telecommunications, and non-linear optical materials. Many researchers have examined the optical, thermal, and structural attributes of tellurite glass matrices in a variety of compositions, including: K_2O–WO_3–TeO_2 (Ersundu et al. 2017), K_2O–Na_2O–TeO_2 (Bahgat and Abou-Zeid 2001), GeS_2–Ga_2S_3–KCl (Haizheng et al. 2004), TeO_2–K_2O–Nb_2O_5 (Tolga Gorgulu et al. 2012), K_2O–TeO_2 (Akagi et al. 1999), GeS_2–In_2S_3–KCl (Haizheng et al. 2006), K_2O–TeO_2–WO_3–B_2O_3 (Edukondalu et al. 2019), TeO_2–V_2O_5–K_2O (Farahmandjou and Salehizadeh 2013), K_2O–Na_2O–Nb_2O_5–TeO_2 (Jeong

et al. 2006). These investigations provide valuable insights into the structural arrangement, dielectric properties, and optical behavior of tellurite glasses with these specific compositions. This work aims to explore the effects of KCl on the structural, optical, and dielectric features of 60 TeO_2-(25−x)Bi_2O_3-15B_2O_3-xKCl glasses, as no prior research has been published on these glass systems.

2 Experimental

The glass compositions examined in this work are of the following form 60TeO_2-(25−x) Bi_2O_3-15B_2O_3-xKCl (x ranging from 0 to 20 mol%). The composition of the materials used and the corresponding codes for the prepared samples are given in Table 1. As the concentration of KCl in the composition increases, a corresponding component of Bi_2O_3 is eliminated from the glass sample. The melt-quenching method was used to synthesize these samples. The required amounts of B_2O_3 (99.9%), Bi_2O_3 (99.98%), TeO_2 (99%), and KCl (99%) of Analar grade were mixed until a finely powdered combination was obtained.

The mixtures were put in porcelain crucibles within an electrically heated furnace operating under normal atmospheric conditions for an hour at a temperature of between 800 and 840 °C to ensure the homogeneity of the molten mixture. After quickly pouring the molten liquids into stainless steel plates, they were allowed to cool naturally to room temperature. The following step involved annealing the glass samples, which is a two-hour process that entails heating them to 200 °C and then lowering them gradually to room temperature. Reducing internal mechanical stress was the goal of the annealing procedure. Following this, the glass samples were carefully cut and polished to produce pieces that had two parallel surfaces, which made optical measurements simpler. By applying the Archimedes principle, the density of the glasses was precisely calculated to within ± 0.001. This required using xylene (0.86 g/cc) as the buoyant liquid. X-ray diffraction (XRD) investigations utilizing a Rigaku table-top system and CuKα radiation confirmed the amorphous character of the glasses. With a step size of 0.02°, the diffractometer was calibrated to cover 2θ angles between 20° and 80°. The prepared samples' glass transition temperature was ascertained through the use of differential scanning calorimeter (DSC) analysis. This is done by differential scanning calorimeter model discovery 25/TA instruments waters at a heating rate of 20 °C/min and a specified range of 50 °C to + 500 °C are used to separate complex thermal events as well as possible. field emission scanning electron microscopy (FESEM) makes it easier to observe materials in extremely fine detail i.e. high resolution and with adequate focus across a wide range of specimen surfaces. Clear images of specimens ranging from things visible to the unaided eye to structures spanning a few nanometres were recorded with the FESEM device SU8010 series made by Hitachi, Japan. Energy-dispersive X-ray (EDX)-7200 analyzers are used to determine elements and provide their quantitative compositional data. FTIR spectrometer modal spectrum two perkin elmer with a wavelength range 4000–400 cm^{-1} was used to record the FTIR spectra of the prepared glass samples. The FTIR spectra of the examined glass samples showed broad peaks made up of several overlapping peaks. The glass samples are fully mixed with dry KBr before being shaped into pellets under 8–10 tones of pressure, ensuring accuracy and repeatability in IR spectrum measurements. An analytical method called Raman spectroscopy uses scattered light to quantify a sample's vibrational energy modes. Raman spectra was recorded using WITec's Alpha 300 Raman spectrometer having laser ranging wavelengths from 532 to 785 nm and a scanning range 4000–100 cm^{-1}. Diffuse reflectance in UV-Vis is a popular and fundamental spectrophotometric method for analyzing powdered glass samples.

The basic principle behind a diffuse reflectance spectrometer is to collect diffusely reflected light and then use a spectrometer to examine its spectrum. A UV-VIS-NIR double-beam spectrophotometer (Shimadzu UV-1601) with a wavelength range of 200–1000 nm was used to record the transmission spectra.

3 Results and discussions

3.1 Physical properties

Using the Archimedes method, the density (ρ) of the glass samples was determined at room temperature. xylene was used as the immersion fluid (Rani et al. 2018a).To minimize error, the ρ of every glass sample was ascertained by utilizing three distinct pieces, and a mean value was considered. The density readings values are accurate to within ± 0.001 g/cm^3. The glass samples were measured twice: once in the immersion liquid (W_L) which has a density of $\rho_a = 0.865$ g /cm^3 and once in the air (W_a). The following formula was used to calculate the glasses' density (Ahamad and Varma 2006):

$$\rho = \rho_a \times \frac{W_a}{W_a - W_L} \tag{1}$$

The kind of glass structure, the percentage of constituent elements, and the molecular weight all affect the density of prepared glasses. The density of the glass samples decreases with increasing KCl content as indicated in Table 1. This decrease could be explained by the fact that the density of Bi_2O_3 (bismuth(III) oxide) is larger (8.90 g/cm^3) than that of KCl (1.984 g/cm^3). The addition of KCl to the present glass system may partially replace the bismuth oxide. Through the breakdown of new bonds, the addition of KCl to the glass upsets the existing network structure. Breaking of connections like the Te–O–Te bond results from this disruption, which creates extra oxygen atoms with a single link to the glass network. Dopant materials such as KCl bring an increase in the amount (NBO) in the glass structure. The presence of NBOs helps the glass structure's free space to expand (Kundu et al. 2013; Rani et al. 2018a).

Molar volume (M_v) and crystalline volume (C_v) has been computed using Eqs. (2 and 3), which can be found in the published work (Berwal et al. 2017):

$$M_V = \frac{\sum_i x_i m_i}{\rho} \tag{2}$$

Table 1 Glass compositions and density

Glass samples code	Composition (mol%)				Density ($\rho \pm 0.001$) (gm/cm^3)
	TeO_2	Bi_2O_3	B_2O_3	KCl	
TBK0	60	25	15	0	6.127
TBK5	60	20	15	5	5.822
TBK10	60	15	15	10	5.489
TBK15	60	10	15	15	5.057
TBK20	60	5	15	20	4.556

where the molecular weight of the ith component is m_i, the molar proportion is x_i, and the sample density is ρ. The molar volume of the prepared glass samples decreases with the systematic replacement of Bi_2O_3 by KCl. This can be because of the smaller bond length and ionic radii of B_2O_3 and KCl as compared to Bi_2O_3. The smaller dimensions of B_2O_3 and KCl result in a reduction of the excess free volume within the glass matrix, thus decreasing the overall molar volume of the glass sample. Similar types of behavior in the molar volume have been observed by other researchers (Kundu et al. 2013, 2014).

$$C_V = \sum_i x_i y_i \tag{3}$$

such as y_i is the ith component, these values indicate the volume occupied by one mole of each substance in its crystalline form. The relationship between M_v and C_v is significant for characterizing glassy materials. When the molar volume of a glass M_v exceeds its crystalline volume C_v (Fig. 1) it suggests the presence of excess structural volume within the glass sample. The calculated values of M_v and C_v are shown in Table 2. This excess volume is

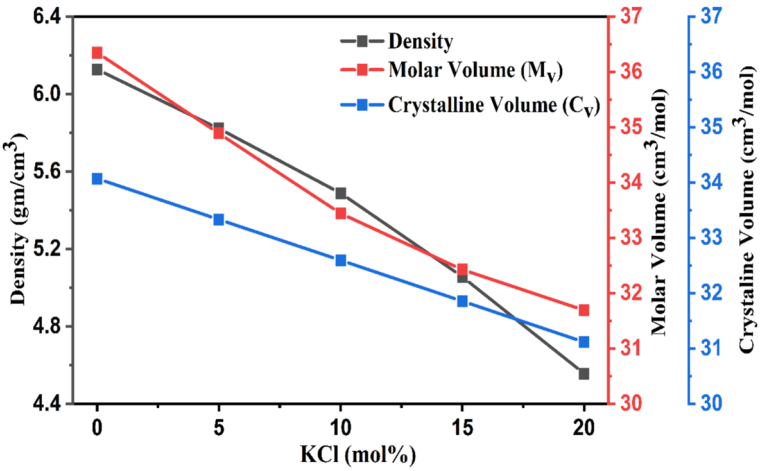

Fig. 1 Variation of density, M_v, and C_v with KCl concentration (mol%) of $60TeO_2$-$(25-x)Bi_2O_3$-$15B_2O_3$-xKCl glass series

Table 2 Physical parameters of $60TeO_2$-$(25-x)Bi_2O_3$-$15B_2O_3$-xKCl glass series

Parameters	TBK0	TBK5	TBK10	TBK15	TBK20
M_v (cm^3/mole)	36.348	34.891	33.442	32.426	31.694
C_v (cm^3/mole)	34.073	33.335	32.595	31.856	31.118
OPD (gm-atm/l)	66.03	64.48	62.79	60.14	56.79
T_g (°C)	376	332	324	310	302
$N_i \times 10^{21}$ (ions/cm^3)	0	0.86	1.80	2.79	3.80
$R_i \times 10^{-7}$ (cm^{-1})	0	1.050	0.822	0.711	0.641
$R_P \times 10^{-8}$ (cm^{-1})	0	4.233	3.312	2.864	2.582
$F_c \times 10^{15}$ (cm^{-2})	0	0.106	0.173	0.232	0.285

a characteristic feature of glassy materials and distinguishes them from their crystalline counterparts (Kundu et al. 2014).

To determine how dense the oxide network is, glass samples' oxygen packing density (OPD) is computed and given by the relation (Ersundu et al. 2017).

$$\mathrm{OPD} = 1000 \times \frac{\mathrm{n} \times \mathrm{density}}{M} \tag{4}$$

The number "n" at this place denotes the quantity of oxygen molecules in a formula unit. M represents the molecular weight of the sample. When KCl is added to the glass composition, chlorine atoms substitute for oxygen atoms in the oxide network. Since chlorine is replacing oxygen, the number of oxygen atoms decreases in the glass samples. This reduction in oxygen content leads to a less densely packed oxide network, resulting in a decrease in OPD values as shown in Table 2 (Berwal et al. 2015).

Equation (5) is used to measure the ionic concentration (N_i). The entry of the dopant KCl into the glass network causes a rise in the ionic concentration (N_i) as shown in Table 2 (Ibrahim et al. 2022).

$$N_i = \frac{\rho \times N_A \times (\mathrm{Mol}\ \%\ \mathrm{of\ dopant})}{Molar\ weight} \tag{5}$$

Equation (6) can be used to estimate the positive correlation between molar volume and interionic distance (R_i) (Rani et al. 2023)**.**

$$R_i = \left(\frac{1}{N_i}\right)^{\frac{1}{3}} \tag{6}$$

Polaron radius (R_P) computed by using the Eq. (7) (Abdelghany et al. 2024; Kaushik et al. 2023).

$$R_P = \frac{1}{2}\left(\frac{\pi}{6N_i}\right)^{\frac{1}{3}} \tag{7}$$

A larger cation field strength (F_c) computed using Eq. (8) (McGlashan et al. 2024)

$$F_c = \left(\frac{Z}{R_P^2}\right) \tag{8}$$

Table 2 appears to provide an overview of the different computed values for N_i, polaron radius (R_P), interionic separation (R_i) and cation field strength (F_c). R_i and R_P perhaps relate to particular traits or attributes of the glass substance. This drop-in R_i and R_P values is thought to be caused by an increase in polarizability brought on by the higher K^+ ion content linked to the elevated KCl level. The ability of atoms or ions in a material to produce induced dipoles in response to an electric field is known as polarizability. More polarization within the glass system is caused by a greater cation field strength (F_c) (Ibrahim et al. 2022; Rani et al. 2023; Kaushik et al. 2023; McGlashan et al. 2024).

3.2 Thermal properties

For investigating the thermal behavior of the materials, Glass transition temperature (T_g) is measured using differential scanning calorimetry (DSC) at temperatures ranging from 50 to 450 °C (Al-Ghamdi et al. 2021). Using this technique, consistent heating of powdered glass samples is carried out while the temperature-dependent heat flux into and out of the sample is observed. The glass transition temperature (T_g) was estimated from the minima that occurred in the graph of dH/dT versus temperature. This temperature indicates the point at which the material begins to transition from a glassy to a rubbery state. (Hussein et al. 2022). The DSC plots of the synthesized glass samples are shown in Fig. 2 and the associated values of T_g are tabulated in Table 2. The observed T_g values may vary depending on the heating rate of 5 °C/min utilized in the DSC investigation. A slower rate of heating makes it possible to determine T_g more precisely because it gives the material enough time to proceed through the glass transition without being affected by kinetic effects (Kundu et al. 2014). Researchers demonstrated that treating tellurite glasses with alkali ions such as K, Na, and Li reduces network connectivity while strengthening connections. This causes T_g to decrease as KCl increases (Ersundu et al. 2017). However, T_g additionally represents the glass network's connection and binding strength. Moreover, T_g usually falls off as the glass's connection and bond strength decline (Edukondalu et al. 2019). A gradual increase in the concentration of non-bridging oxygen (NBO) atoms is implied by the reduction in T_g with increasing KCl content. The addition of KCl causes structural alterations that result in a less densely packed and more flexible glass network. The correlation between T_g and oxygen packing density (OPD), is depicted in Fig. 3. In tellurite glasses with high TeO_2 concentration, the fundamental structural units consist of TeO_4 trigonal bipyramids. These units feature a lone pair of electrons occupying one of the equatorial positions, and most tellurium atoms are connected at their vertices through a lone pair of electrons (Lee et al. 2008). The Te–O_{eq} and Te–O_{ax} bonds are weakened, and the TeO_4 trigonal bipyramid network disintegrates upon the addition of an alkali ion to tellurite glass. This results in the emergence of non-bridging oxygen (NBO) atoms in both the Te–O_{eq} and Te–O_{ax} connections (Akagi et al. 1999). Tellurite-based glasses with an alkali ion as a modifier experience a structural change in the coordination polyhedron as a result of the variation in KCl

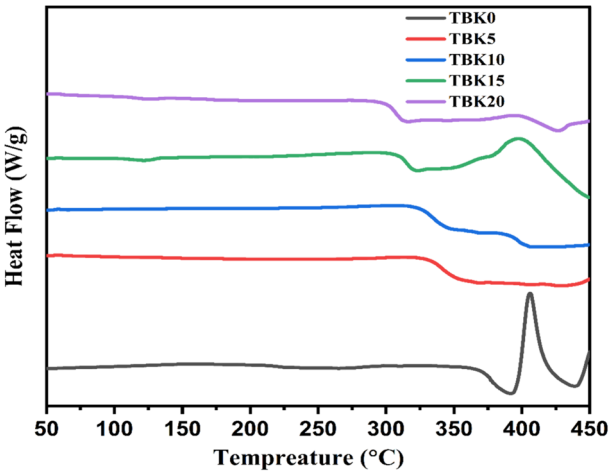

Fig. 2 DSC patterns of $60TeO_2$-$(25-x)Bi_2O_3$-$15B_2O_3$-xKCl glass system

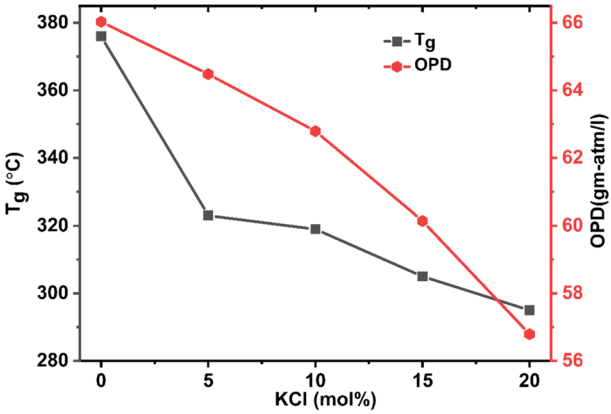

Fig. 3 Variation of T_g and (OPD) with KCl content (mol%) for $60TeO_2$-$(25-x)Bi_2O_3$-$15B_2O_3$-xKCl glass system

content (Sidkey and Gaafar 2004; Hussein et al. 2022). Tellurite glasses produce four and three-coordinated tellurium polyhedra at the same time. TeO_4 polyhedra change into TeO_3 polyhedra due to the action of the alkali ion modifier. This change of the TeO_4 trigonal bi-pyramid into the TeO_3 trigonal pyramid increases with the alkali ion modifier increase. The extra TeO_3 trigonal pyramidal groups' electron pairs do not get along well with one another (Poria et al. 2024; Wang et al. 2013).

3.3 Structural properties

3.3.1 XRD

By analyzing the XRD patterns, gain valuable insights into the crystalline or non-crystalline nature of the material. The generated glasses' amorphous or non-crystalline nature is confirmed by the XRD patterns (Fig. 4) which show a wide hump in the 20°–40° region for 2θ values. Information regarding the angles at which the sample diffracts X-rays is

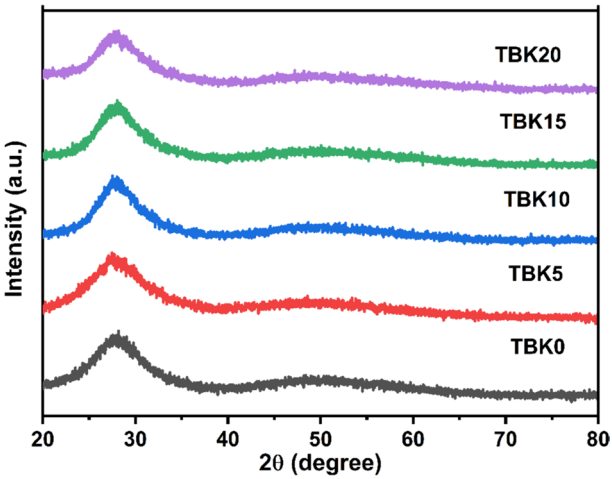

Fig. 4 XRD patterns of $60TeO_2$-$(25-x)$ Bi_2O_3-15 B_2O_3-xKCl glass system

provided by the scattering angles in the XRD pattern, which are represented by the 2θ values. This observation is consistent with the usual structural characteristics of glassy materials in which there is a lack of regularity and order in the arrangement of atoms, as opposed to crystalline structures (Rani et al. 2018b).

3.3.2 EDX and FESEM analysis

The high-resolution imaging method known as field emission scanning electron microscopy (FESEM) is used to examine a sample's morphology-the size and form of the particles as well as its topography at a resolution of nanometers. When used in conjunction with energy dispersive X-ray spectroscopy (EDX) any object's elemental makeup can be revealed under investigations in addition to its distribution. The element composition of a region as small as a few nanometer diameters can be studied using EDX elemental composition, which can be quantitatively reported as weight % or atomic percentage (Abdelhameed et al. 2019; Sekhar et al. 2020). Figures 5 and 6 display the EDX spectrum and the FESEM image of the TBK10 glass surface respectively. The flawless and uniform surface seen in the TBK10 glass's FESEM image confirms the material's amorphous structure as well as supports the results of other analytical methods like X-ray diffraction. The elemental plots of the substance under examination can be learned a great deal from the (EDX) spectrum displayed in Figs. 5 and 7, as well as the accompanying bar chart that shows the weight percentage of each element. Tellurium (Te), potassium (K), bismuth (Bi), chlorine (Cl), and oxygen (O) are among the elements that can be found in the spectrum. Tellurium (Te) is the major element in the material's composition, as indicated by its higher weight % when compared to other elements in the EDX analysis. This is consistent with the composition that is expected for tellurite glasses, where tellurium usually makes up a sizable component of the glass matrix. Chlorine (Cl) is comparatively low in weight percentage, indicating that its abundance is lower than that of other elements. Cl comprises only 0.54 mol% of the composition, according to the EDX study, which explains the low weight percentage seen in the bar chart (Fig. 7).

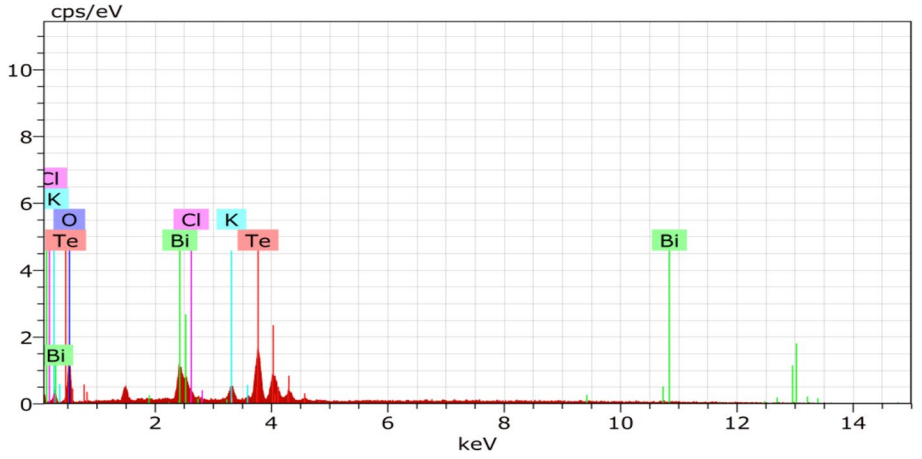

Fig. 5 EDX spectra showing elemental maps of the components in the 60 TeO_2-15 Bi_2O_3-15B_2O_3-10KCl glass samples

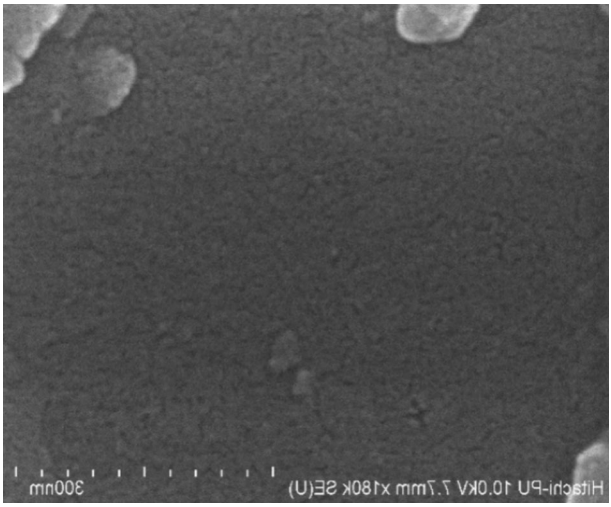

Fig. 6 FESEM image of $60TeO_2$-$15Bi_2O_3$-15 B_2O_3-10KCl a glass sample

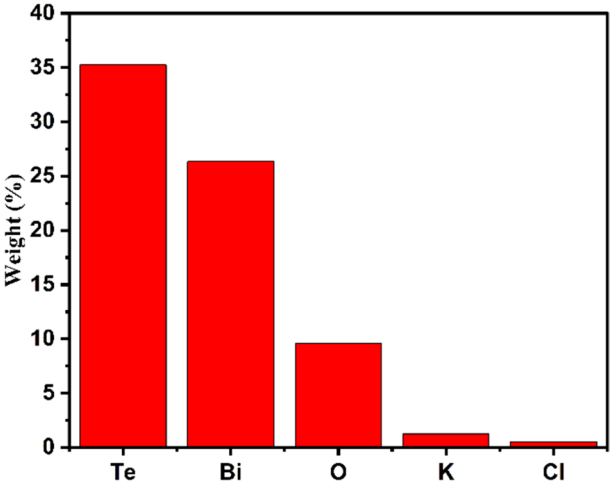

Fig. 7 EDX bar chart displaying the percentage and elements maps of the $60TeO_2$-$15Bi_2O_3$-$15B_2O_3$-10KCl glass sample

3.3.3 FTIR analysis

In FTIR analysis, molecules absorb infrared radiation at specific frequencies leading to characteristic absorption bands in the spectra**.** These absorption bands reveal the samples under analysis of molecular structure and functional groups. The FTIR spectra obtained for the glass system are generally represented graphically (Fig. 8) which shows the strength of absorption as a function of wavenumber (frequency) in the 400–1500 cm^{-1} range at room temperature. The spectra's broad bands are divided into several symmetrical Gaussian bands by deconvolution. Specialized software such as Origin helps to fit the experimental data with Gaussian functions to resolve overlapping peaks and extract relevant information about the composition and structure of the glass material. The distribution of these peaks and their associated characteristics are shown in Fig. 9, which shows the

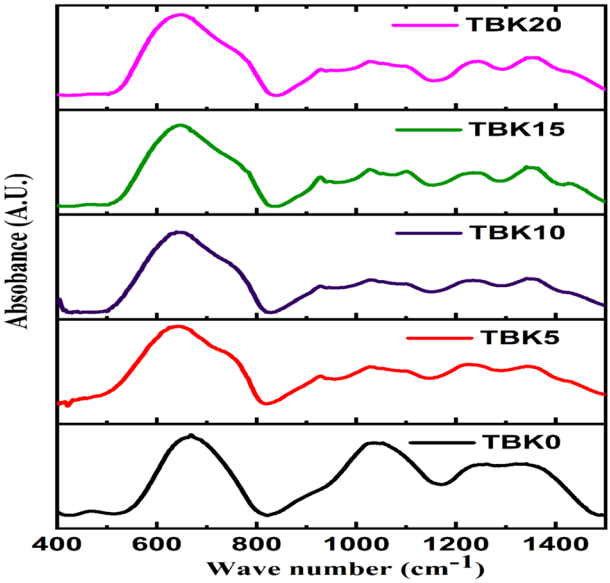

Fig. 8 FTIR spectra of $60TeO_2$-(25−x) Bi_2O_3-15 B_2O_3-xKCl glass system

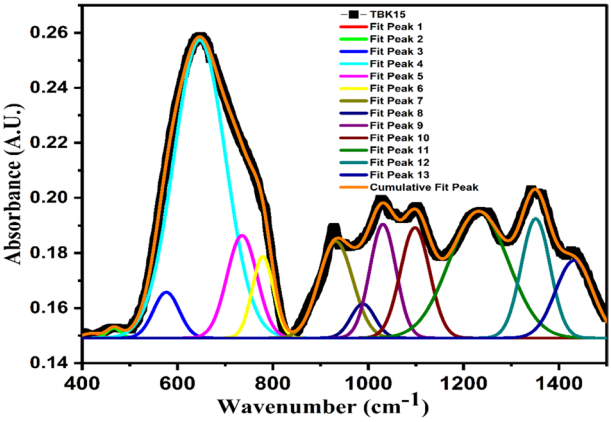

Fig. 9 Deconvoluted FTIR spectra of $60TeO_2$-10Bi_2O_3-15B_2O_3-15KCl glass system

FTIR data fitting for TBK15 samples. A detailed list of the peaks seen in the deconvoluted FTIR spectra of these samples is given in Table 3. The concentration or abundance of particular functional groups or molecular species within the sample by calculating each peak's relative area (A). Furthermore, the full width at half maximum (W_h) displays each peak's spectrum resolution and width. In contrast, the peak position (X_p) offers information about the nature of molecular vibrations connected to specific structural motifs or chemical interactions. Table 4 is a reference for comparing observed band placements in FTIR spectra to their matching infrared (IR) band assignments. The IR spectra show four primary bands in the ranges of 415–480 cm^{-1}, 500–800 cm^{-1}, 873–916 cm^{-1}, 916–1185 cm^{-1} and 1209–1444 cm^{-1} across all glass series.

Table 3 Peak position (X_p), peak area (A) and full width at half-maxima (W_h) of deconvoluted peaks of FTIR spectra of the glass series 60 TeO2-(25−x) Bi2O3-15 B2O3-x KCl

Peak no	TBK0			TBK5			TBK10			TBK15			TBK20		
	Xp (cm^{-1})	A (a.u.)	W_h (cm^{-1})	Xp (cm^{-1})	A (a.u.)	W_h (cm^{-1})	Xp (cm^{-1})	A (a.u.)	W_h (cm^{-1})	Xp (cm^{-1})	A (a.u.)	W_h (cm^{-1})	Xp (cm^{-1})	A (a.u.)	W_h (cm^{-1})
1	**415**	0.3	39.9	**433**	0.6	38	**404**	0.3	7.2	**419**	0.1	45	**409**	0.1	42
2	**480**	1.7	46	**475**	0.9	46	**413**	0.7	78	**466**	0.1	34	**465**	0.1	42
3	**592**	0.8	70.9	**572**	10	104	**579**	8.3	90	**576**	1.1	63	**578**	2	64
4	**619**	8	68	**645**	18	108	**654**	33	121	**646**	15	128	**646**	16	122
5	**683**	6.1	96.6	**711**	8.5	103	**739**	7.2	69	**735**	3	74	**738**	4.5	84
6	**753**	1.1	51.8	**757**	4.7	63	**776**	2.8	45	**779**	1.7	52	**781**	1.5	50
7	**873**	0.6	69.6	**886**	1.0	47	**928**	8.8	100	**932**	3.1	84	**933**	3.6	88
8	**916**	1.7	96.4	**919**	3.7	67	**1020**	10.5	96	**989**	0.8	58	**981**	0.6	47
9	**1048**	7.9	173	**1033**	16	149	**1104**	5	73	**1031**	2.8	65	**1023**	2.3	61
10	**1209**	5.9	134	**1110**	1.4	61	**1185**	6	106	**1098**	4.0	72	**1090**	5	103
11	**1282**	0.1	15.9	**1230**	17	149	**1252**	9.7	105	**1232**	7.2	146	**1236**	5.7	101
12	**1328**	5.5	156	**1344**	5	86	**1348**	9	87	**1351**	3.3	72	**1352**	6	98
13	**1384**	0.2	17.6	**1420**	8.7	142	**1435**	7	112	**1432**	2.7	92	**1444**	2.7	92

Bold numbers represent the peak position (X_p) of the deconvoluted spectra

Table 4 IR spectra wave number and band assignments for the glass series $60TeO_2$-(25−x) Bi_2O_3-15 B_2O_3-xKCl

Wavenumber (cm^{-1})	IR band assignments	References
415–480	Stretching and bending vibrations exhibit symmetry because of the corner sharing of TeO_{3+1} polyhedral, TeO_4, and TeO_3 units in the Te–O–Te connection	Kundu et al. (2016)
500–800	TeO_2 is the main framework	Dhankhar et al. (2016)
572–592	anti-symmetric stretching vibrations of Te–O bonds of TeO_4 structural units	Rani et al. (2018b)
619–654	symmetric stretching vibrations Te–O bonds inTeO_4 and TeO_3 structural units	Berwal et al. (2015)
683–739	Te–O (non-bridging) stretching vibration in TeO_3 structural unit	Bahgat and Abou-Zeid (2001)
753–781	stretching vibration Te–O (non-bridging) in TeO_3 and TeO_6 structural units	Ersundu et al. (2017)
873–916	symmetrical Bi–O vibrations in BiO_3 units	Gupta et al. (2017)
916–1030	B–O stretching from diborate groups in BO_4 units	Al-Ghamdi et al. (2021), Rani et al. (2018a)
1031–1185	B–O stretching mode from tri, tetra, and penta borate groups in BO_4 units	Rammah et al. (2019), Al-Ghamdi et al. 2021)
1209–1282	B–O stretching vibrations of trigonal BO_3 units in boroxol rings	Saritha et al. (2008, Singh et al. (2014)
1328–1444	B–O–B vibrational modes in metaborate, pyroborate and orthoborate groups of BO_3 triangular units	Saritha et al. (2008), Thakur et al. 2016)

The detection of an IR band between 414 and 480 cm^{-1} in all glass samples, is attributable to stretching and bending vibrations with symmetry of Te–O–Te connections (Kundu et al. 2016). A common structural motif in these glasses is revealed by the occurrence of infrared peaks in the 500–800 cm^{-1} spectral region in all glass samples which are attributable to the presence of tellurium dioxide (TeO_2) acting as the major framework material (Dhankhar et al. 2016). Peaks in the infrared (IR) spectrum at 572–592 cm^{-1} indicate anti-symmetric stretching vibrations of tellurium–oxygen (Te–O) bonds within TeO_4 structures (Rani et al. 2018b). The IR band at 619–654 cm^{-1} may be due to symmetry stretching vibration Te–O bonds in the arrangement of oxygen and tellurium atoms in the TeO_4 and TeO_3 structural units (Berwal et al. 2015). The occurrence of an IR band between 683 and 739 cm^{-1} may be attributed to Te–O (non-bridging) stretching vibrations in the TeO_3 trigonal pyramids (tp) structural units (Bahgat and Abou-Zeid 2001). The TeO_3 and TeO_6 structural units' stretching vibrations, which are non-bridging, may be linked to the infrared band seen at approximately 753–781 cm^{-1} (Ersundu et al. 2017). The peaks observed at 683 cm^{-1} and 753 cm^{-1} for sample x = 0 (TBK0) indicate a little shift towards a higher wavenumber as the KCl content increases. In addition, even as the peak TeO_4 intensity at roughly 650 cm^{-1} improves, there is an apparent rise in the intensity of the TeO_3 and TeO_{3+1} peak within the range of 683–739 cm^{-1}. The reason for this shift can be attributed to the transformation of TeO_4 units into TeO_3 and TeO_{3+1} units, leading to an overall increase in the quantity of TeO_3 units within the glass network.

The symmetrical stretching vibration of the bismuth-oxygen (Bi–O) bonds inside the BiO_3 units explains the shoulder-shaped peak observed in each glass sample at 873–916 cm^{-1} (Gupta et al. 2017). It indicates the presence of Bi^{3+} ions with non-bridging oxygen in the form of $[BiO]^-$ defects in all glass compositions. The infrared band observed in the 916–1185 cm^{-1} range has been connected to the B–O stretching vibrations within tetrahedral BO_4 units (Al-Ghamdi et al. 2021). For x = 15 (TBK15), the three component peaks that comprise this band are located at 989, 1031, and 1098 cm^{-1}. The stretching vibrations of the boron–oxygen (B–O) bonds within the BO_4 units, which originate from di-borate groups, ultimately establish this infrared (IR) peak at 989 cm^{-1} (Rani et al. 2018a). A shift to 981 cm^{-1} in the peak's center has been observed, and this movement is associated with a substitution of KCl in place of Bi_2O_3. This observation implies that the presence of KCl raises the number of BO_4 units inside the glass network. Peaks at 1031 cm^{-1} and 1098 cm^{-1} in the infrared (IR) spectrum are caused by the stretching vibrations of boron–oxygen (B–O) bonds inside tri-, tetra- and penta-borate units inside the BO_4 unit (Rammah et al. 2019).

It has been noted that the center of these peaks shifts to lower wavenumbers with decreasing Bi_2O_3 content. The band found in the 1200–1500 cm^{-1} range is thought to be caused by the B–O stretching vibrations bonding in the BO_3 trigonal structural units (Saritha et al. 2008). The B–O stretching vibrations for the boroxol rings inside the trigonal BO_3 units can be linked to the wide range of component peaks that ranged from 1209 to 1282 cm^{-1} (Singh et al. 2014). The peaks observed in the 1328–1444 cm^{-1} range are caused by the stretching vibrations of trigonal BO_3 units, which are found in the orthoborate, pyroborate, and metaborate groups (Thakur et al. 2016). The peak found at 1282 cm^{-1} in the glass TBK0 sample has been seen to shift to 1232 cm^{-1} as KCl concentration rises. This alteration suggests a little conversion of BO_3 trigonal units into BO_4 tetrahedral units. The peak at 1432 cm^{-1} shifts to lower wavenumbers, which suggests that there are more BO_3 units present.

An FTIR analysis reveals no vibrational modes associated with K^+ cations. These results imply that K^+ ions occupying modifier sites within the glass network are progressively

growing so K^+ cations may function as network modifiers. The amount of TeO_4 groups decreases in proportion to an increase in KCl concentration. This is because certain TeO_4 structural units change into TeO_3 units, which lowers the bismuth concentration. This demonstrates that NBOs are produced when KCl concentration rises (Al-Ghamdi et al. 2021; Lee et al. 2008). Bismuth is present in all samples as BiO_3 pyramidal structural units. The breakdown of specific six-membered boroxol units structural arrangements made up of both trigonal BO_3 and tetrahedral BO_4 units is observed. The FTIR spectra are consistent with the glass transition temperature (T_g), implying that the addition of KCl may have introduced structural defects and unpredictability into the glass system.

3.3.4 Raman analysis

Figure 10 depicts the Raman spectra of the glass samples which reveal many bands corresponding to different vibrational modes. These spectra's deconvolution assists in locating particular vibrational modes and the accompanying Raman shifts. A deconvoluted spectrum for the glass sample $60TeO_2$-$(25-x)Bi_2O_3$-$15B_2O_3$-xKCl is shown in Fig. 11. Because glasses are non-crystalline, there is likely intrinsic structural disorder, as indicated by the growing range of peaks seen in the spectra of all the glass samples. Tables 5 and 6 provide detailed information on the band placements, their corresponding Raman band assignments, and values such as whole width at half maximum (W_h), amplitude (A), and peak position (X_p). These details are crucial for understanding the structural characteristics and behavior of the glass system under study.

Two main groups may be identified from the Raman spectra obtained in the range of 100–1600 cm^{-1}; the cations of heavy metals are represented by those below 650 cm^{-1}, while the borate network is represented by those above 650 cm^{-1} (Dhankhar et al. 2016). The Raman spectra are composed of five peaks at approximately 80–181 cm^{-1}, 260–380 cm^{-1}, 403–444 cm^{-1}, 496–570 cm^{-1} and 608–635 cm^{-1} while three strong peaks at approximately 660–672 cm^{-1}, 745–761 cm^{-1} and 854–895 cm^{-1} respectively. The peak of the Raman spectra observed at 80–181 cm^{-1} is associated with the acoustically-like vibrational modes that are linked to the organized micro-regions within the glass (Kundu et al. 2016). The band observed at about 260–318 cm^{-1} is caused by the Bi–O unit vibrations

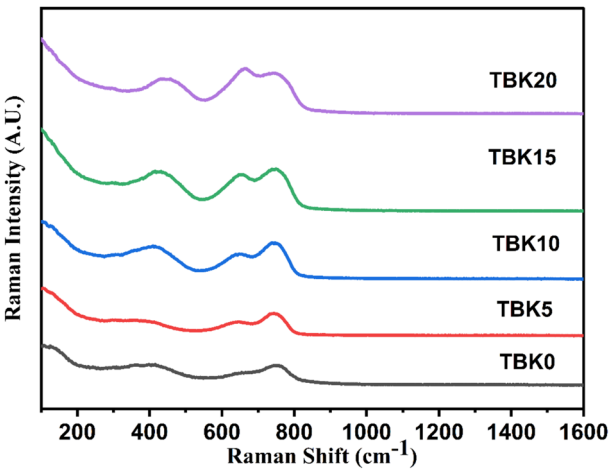

Fig. 10 Raman spectra of $60TeO_2$-$(25-x)Bi_2O_3$-$15B_2O_3$-xKCl glass system

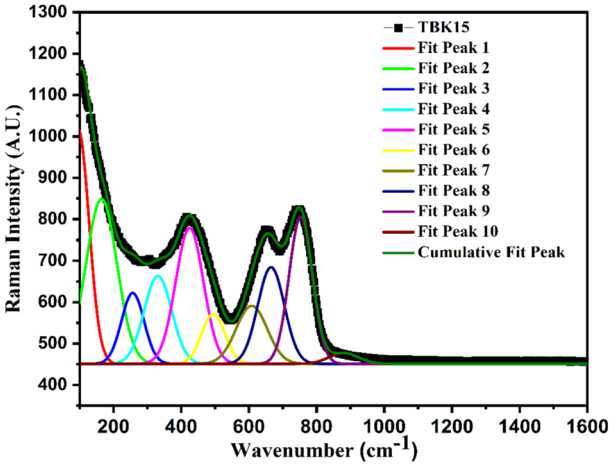

Fig. 11 Deconvoluted Raman spectra of $60TeO_2$-$10Bi_2O_3$-$15B_2O_3$-15KCl glass system

that are present in both BiO_6 and BiO_3 configurations (Singh et al. 2014). The prominent peak observed at 329–380 cm^{-1} in the spectra is attributed to stretching vibrational modes of Bi–O–Bi movements in deformed BiO6 octahedral units (Kundu et al. 2014). The peak shifts towards the higher wavenumber side and becomes less prominent as the amount of KCl in the glass matrix increases. TeO_2-rich TeO_3 pyramids and TeO_4 bipyramids are organized in a trigonal pattern. The main cause of the stretching vibrations observed in tellurite glasses is the structural units of TeO_4 and TeO_3. Asymmetric stretching and bending vibration resulting from the corner sharing of TeO_{3+1} polyhedral, TeO_4, and TeO_3 units with the Te–O–Te connections may be the cause of the Raman signal observed at 403–444 cm^{-1} in all glass samples (McGlashan et al. 2024).

Within TeO_4 structural units, tellurium atoms with four coordination exhibit Raman peaks between 496 and 570 cm^{-1} in all glass samples (Wang et al. 2013). These peaks are most likely the result of Te–O–Te bridges. Furthermore, all glass samples exhibit a Raman band with a wavelength between 608 and 635 cm^{-1} which is associated with the symmetry stretching vibrations of Te–O bonds lying in the axial direction ($Te–O_{ax}$) inside the TeO_4 structural groups (Akagi et al. 1999). The Raman band between 660 and 672 cm^{-1} is assigned to Te–O stretching vibrations of TeO_3 trigonal pyramids (Alshamari et al. 2023). The band's intensity progressively increases with KCl content, indicating that TeO_4 units undergo a transition to TeO_3 units through the TeO_{3+1} intermediate coordination. Furthermore, Te–O bending vibrations within the TeO_3 and TeO_6 structural units may have been the source of the Raman band, which was detected in all glass samples and had a wavelength ranging from 745 to 761 cm^{-1} (Sidkey and Gaafar 2004). Structure changes inside the glass network account due to the observed variations in these peaks which exhibit dramatic intensity shifts from lower to higher wavenumbers. This suggests that as KCl levels rise, non-bridging oxygens atoms contribution increases. When alkali oxides, heavy metal, and alkaline earth ions are added to TeO_2-rich glass compositions, the glass network grows upward, and non-bridging oxygen species form. TeO_4 structural units are transformed into TeO_{3+1} polyhedra as a result of this inclusion and TeO_3 units are also transformed. The metaborate group of BO_3 triangular units contains B–O–B and B–O vibrational modes, as indicated by the peak at 854–895 cm^{-1} (Rani et al. 2018a). As the concentration of KCl in the glass

Table 5 Raman spectra wave number and band assignments for the glass series 60 TeO_2-(25−x) Bi_2O_3-15 B_2O_3-x KCl

Wave number (cm^{-1})	Assignments for Raman bands	References
80–181	Modes of vibration of the organized micro-regions	Kundu et al. (2016)
260–318	Bi–O vibrations in BiO_3 and BiO_6 units	Singh et al. (2014)
329–380	Stretching vibrations in Bi-O-Bi in BiO_6 octahedral units	Kundu et al. (2014)
403–444	Stretching and bending vibrations exhibit symmetry because of the corner sharing of TeO_{3+1} polyhedral, TeO_4, and TeO_3 units in the Te–O–Te connection	McGlashan et al. (2024)
496–570	anti-symmetric stretching vibrations of Te–O bonds of TeO_4 structural units	Wang et al. (2013)
608–635	symmetric stretching vibrations Te–O bonds inTeO_4 and TeO_3 structural units	Akagi et al. (1999)
660–672	Te–O (non-bridging) stretching vibration in TeO_3 structural unit	Alshamari et al. (2023), (Dhankhar et al. (2016)
745–761	stretching vibration Te–O (non-bridging) in TeO_3 and TeO_6 structural units	Sidkey and Gaafar (2004)
854–895	B-O-B vibrational modes in a metaborate group of BO_3 triangular units	Rani et al. (2018a)

Table 6 Characteristics from deconvolution Raman spectra (Xp, A and W_h stands for relative Peak position, peak areas and full width at half maxima respectively) for 60 TeO_2-(25−x) Bi_2O_3-15 B_2O_3-x KCl glass series

Peak no	TBK0			TBK5			TBK10			TBK15			TBK20		
	Xp (cm^{-1})	A(a.u.)	W_h (cm^{-1})	Xp (cm^{-1})	A(a.u.)	W_h (cm^{-1})	Xp (cm^{-1})	A(a.u.)	W_h (cm^{-1})	Xp (cm^{-1})	A(a.u.)	W_h (cm^{-1})	Xp (cm^{-1})	A(a.u.)	W_h (cm^{-1})
1	**100**	195791	174	**106**	32904	88	**103**	38000	85	**95**	45225	75	**80**	75000	110
2	**260**	24351	96	**181**	22036	120	**173**	22992	92	**164**	45938	108	**180**	40000	120
3	**318**	13805	81	**260**	3680	100	**272**	24775	125	**257**	14306	78	**281**	15809	92
4	**380**	28729	106	**329**	11132	98	**358**	13866	90	**332**	21728	96	**366**	19485	112
5	**444**	28466	129	**403**	15119	123	**425**	22946	96	**425**	33790	97	**445**	24250	97
6	**570**	817	98	**531**	3897	100	**501**	8588	110	**495**	10424	81	**496**	8637	83
7	**635**	13649	77	**618**	6209	89	**625**	10991	110	**608**	16106	108	**616**	22753	143
8	**716**	24984	109	**664**	7364	90	**660**	15584	107	**665**	23014	93	**672**	30000	102
9	**755**	10280	61	**745**	14489	71	**748**	23905	75	**753**	30464	81	**761**	26775	82
10	**854**	3101	144	**871**	16069	119	**880**	3296	160	**880**	2840	103	**895**	4717	156

Bold numbers represent the peak position (X_p) of the deconvoluted spectra

matrix rises, these peaks have been observed to shift to the higher wavenumber side and to become less intense. Increase in the concentration of KCl in the glass samples leads to the conversion of TeO_4 structural units into TeO_3 structural units. This implies that higher KCl concentrations promote non-bridging oxygen contributions (Sidkey and Gaafar 2004).

3.4 Optical properties

3.4.1 Optical transmittance and absorbance

The diffuse reflectance spectra (DRS) of the TBK glasses in the wavelength range of 300–800 nm are shown in Fig. 12 and offer important insights into their optical characteristics. One notable finding from the data is that the reflectance rises when potassium chloride (KCl) replaces bismuth oxide (Bi_2O_3) in the glass composition. Materials' optical characteristics, such as their reflectance, absorption, and transmission, are intimately linked to their bandgap and electrical structure. The electronic structure and energy levels of glass can be affected by the addition of KCl, which may change the material's optical properties. There is a clear correlation between KCl content and reflectivity, as seen by the sample with the highest KCl doping (TBK20) showing the highest reflectance and the sample with no KCl doping (TBK0) showing the lowest reflection. The diffuse reflectance spectrum (DRS) shifts to lower wavelengths with increase in KCl content (Farahmandjou and Salehizadeh 2013). The optical phonon confinement in the glass samples is the reason for the rise in reflectivity. The absorbance spectra for each sample, shown in Fig. 13 as α (cm^{-1}) vs wavelength, offer crucial information on the optical characteristics of the TBK glasses. Values of λ_c the wavelength cut-off at which absorbance begins provide information on the materials' band gap energy (E_g).Table 7 tabulates the values of the band gap energy (E_g) of the glass samples which indicates an increase with KCl concentration. This observation indicates that the incorporation of KCl leads to a modulation of the band gap energy of the glasses (Takebe et al. 2007). The absorbance spectrum for sample TBK15, with a corresponding cut-off wavelength (λc) of 366 nm, is shown in Fig. 14.

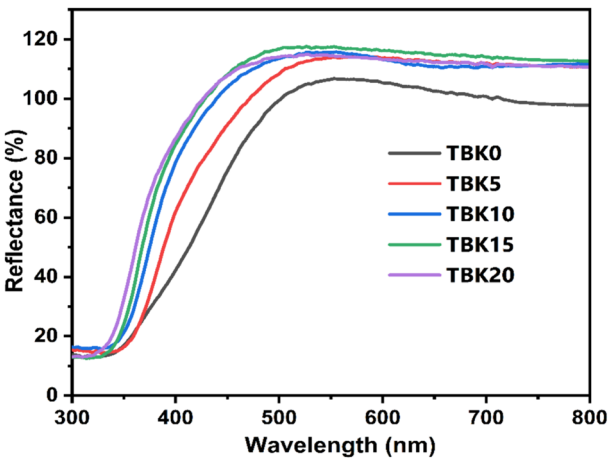

Fig. 12 Reflection spectra of $60TeO_2$-$(25-x)Bi_2O_3$-$15B_2O_3$-xKCl glass system

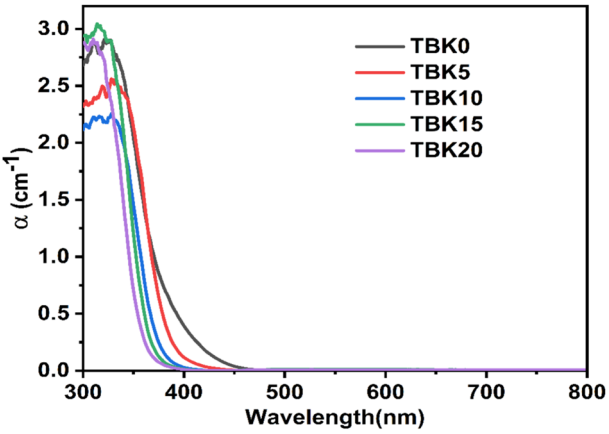

Fig. 13 Optical absorption spectra of $60TeO_2$-$(25-x)Bi_2O_3$-$15B_2O_3$-xKCl glass system

Table 7 Optical parameters for 60 TeO_2-$(25-x)$ Bi_2O_3-15 B_2O_3-xKCl glass series

Variable	TBK0	TBK5	TBK10	TBK15	TBK20
E^1_{opt} (eV) indirect band gap	2.78	3.07	3.16	3.25	3.31
E^2_{opt} (eV) direct band gap	3.37	3.39	3.43	3.51	3.57
E_U (eV)	0.289	0.264	0.245	0.196	0.183
λ_c (nm)	387	381	372	366	359
N	2.46	2.38	2.35	2.33	2.31
R_m $(m^3)*10^{-6}$	22.798	21.221	20.149	19.355	18.801
M	0.373	0.392	0.397	0.403	0.407
α_m	9.047	8.421	7.996	7.680	7.461

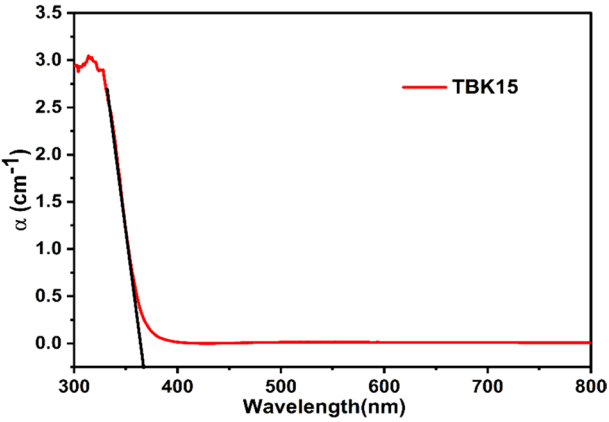

Fig. 14 Optical absorption spectra of $60TeO_2$-$10Bi_2O_3$-$15B_2O_3$-15KCl glass system

3.4.2 Optical band gap

The Kubelka–Munk function F(R) is a widely used method for analyzing diffuse reflectance spectra (Fig. 12) to determine the optical band gap of materials. For materials with

strong scattering or high absorbance, like opaque or powdered samples, the Kubelka–Munk function is especially helpful. When comparing optical properties to a direct measurement of reflectance, it offers a more realistic depiction by taking into consideration both the absorption and scattering of light within the material. The Kubelka–Munk function is defined as (Ibrahim et al. 2022).

$$F(R) = \frac{K}{S} = \frac{(1-R)^2}{2R} \tag{9}$$

where S = 2R is the scattering factor, R is the reflectance and $K = (1-R)^2$ is the molar absorption coefficient. When examining a sample's optical properties, the Tauc plot is a helpful tool for figuring out its optical band gap energy (Kaushik et al. 2023).It involves plotting the quantity $(F(R).h\nu)^{1/r}$ against the photon energy (hv), where $F(R)$ is the Kubelka–Munk function, $h\nu$ is the photon energy, and r is a parameter that defines the characteristics of an optical transition typically set to 1/2 or 2. To determine E_g extrapolate a tangential line to the $h\nu$ axis corresponding to the point where $(F(R).h\nu)^{1/r} = 0$ (Kashif et al. 2018). This intersection point provides an estimate of the band gap energy E_g of the prepared glass samples. This plot demonstrates the band gap energy and the type of optical transitions (direct or indirect) in the glass samples is shown in Figs. 15 and 16.

Relationship between optical band gap E_g and absorption coefficient $(F(R)h\nu)$ in various amorphous materials, as shown by Equation (Rani et al. 2023).

$$(F(R)hv) = B\left(hv - E_g\right)^r \tag{10}$$

The optical band gap energy varies when the KCl content rises from 0 to 20 mol%, accompanied by a decrease in the Bi_2O_3 content, as shown by the Tauc plot in Table 7. To be precise, the indirect band gap rises from 2.78 to 3.31 eV, whereas the direct band gap rises from 3.37 to 3.57 eV. For different types of optical transitions (direct forbidden, indirect forbidden, direct allowed, and indirect allowed), the possible values of r are 1/3, 3, 1/2, and 2, respectively. The choice of r depends on the nature of the electronic transitions occurring in the glasses and B is a constant that is energy-independent. In many glassy materials, particularly those composed of amorphous structures like the ones studied here, the band gaps are often predominantly indirect (Aloraini et al.

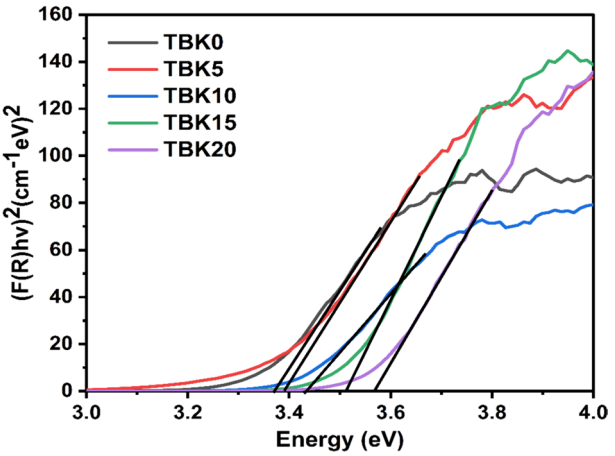

Fig. 15 $(F(R)h\nu)^2$ as a function of photon energy (eV) for the $60TeO_2$-$(25-x)Bi_2O_3$-$15B_2O_3$-xKCl glass system

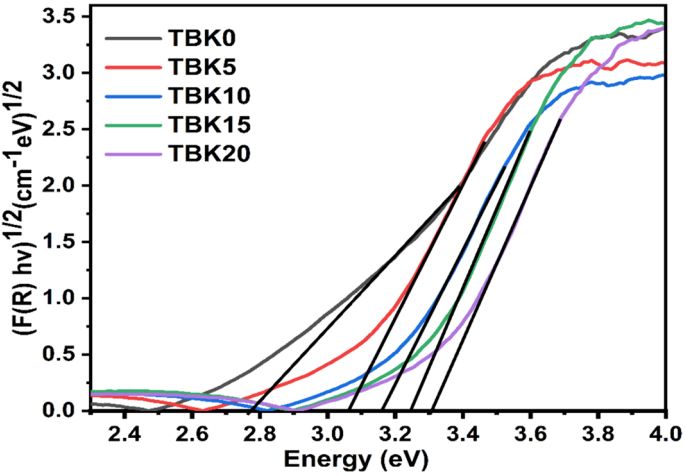

Fig. 16 $(F(R)h\nu)^{1/2}$ as a function of photon energy (eV), for the $60TeO_2$-$(25-x)Bi_2O_3$-$15B_2O_3$-$xKCl$ glass system

2021; Lee et al. 2008; Edukondalu et al. 2019; Farahmandjou and Salehizadeh 2013; Jeong et al. 2006; Ahamad and Varma 2006).

Some structural alterations inside the glass network may be responsible for the increase in the indirect band gap. In comparison with Te–O, Te–Bi, Te–B, and Bi–O bonds, when Bi_2O_3 gets replaced with KCl, the densities of K–Cl, Bi–Cl, B–O and B–Cl bonds might increase. In comparison to Te–O (391 eV), Te–Bi (232 eV), Te–B (354 eV), and Bi–O (343 eV) bonds, bonds like K–Cl (427 eV), Bi–Cl (305 eV), B–O(806 eV) and B–Cl (536 eV) possess substantially greater bond dissociation energies (Ahlawat et al. 2023; Thanigaiselvan et al. 2015). The optical band gap energies are prominence as a function of decreasing bismuth concentration and increasing KCl content. This is due to the increase in the number density of K–Cl, Bi–Cl, B–O and B–Cl bonds with high bond dissociation energy (Poria et al. 2023). This could also account for the blue shift in λ_c values with KCl concentration shown in Table 7. Internal instability in amorphous materials, such as glasses, can fluctuate unpredictably leading to band tailing in the forbidden energy gap.

3.4.3 Urbach energy and refractive index

The Urbach energy (E_U) characterizes the exponential tail of the absorption spectrum in the region near the band edge and provides insights into the extent of the degree of disorder or structural defects within the material, with higher values indicating greater disorder. The function F(R) achieves the same description as the α(v) absorption coefficients. Apply the following calculation (Marzuki et al. 2023).

$$\alpha(v) = B.\exp\left(\frac{hv}{E_U}\right) \tag{11}$$

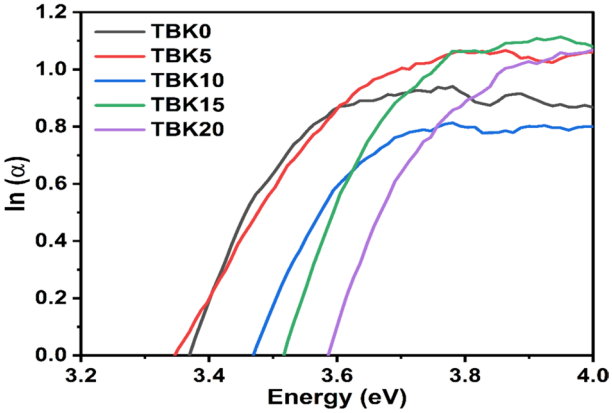

Fig. 17 Urbach plots for $60TeO_2$-$(25-x)Bi_2O_3$-$15B_2O_3$-xKCl glass system

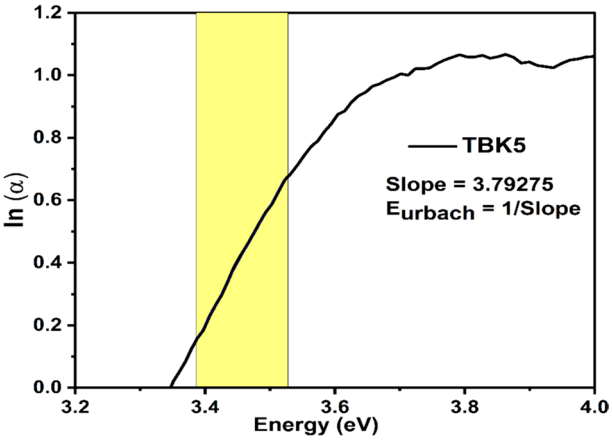

Fig. 18 Urbach plots for $60TeO_2$-$20Bi_2O_3$-$15B_2O_3$-5KCl glass composition

where h is the Planck's constant and v is the photon frequency. E_U is a sample measure of disorderliness and is dependent on several variables, including temperature, lattice thermal vibrations, average photon energy, ionic bond and static disorder. The graph of the natural logarithm of the absorption coefficient (ln(α)) vs photon energy (hv) is shown in Figs. 17 and 18. Urbach energy (E_U) drop from 0.289 to 0.183 eV (Table 7) with increasing KCl concentration in TBK glasses. This implies that the disorderliness or flaws in the samples decrease with increasing KCl content. The optical bandgap of the material decreases as defect levels increase, as evidenced by the rise in Urbach energy. Many researchers have reported similar findings for oxide glasses (Karthika et al. 2023; Pandarinath et al. 2016; Samee et al. 2013).

The mathematical relationship represented by Eq. (12) enables to computation of the refractive index using indirect band gap energy (E_{opt}) proposed by Dimitrov and Sakka (Kundu et al. 2014; Dimitrov and Komatsu 2010).

$$\frac{N^2-1}{N^2+2}=1-\sqrt{\frac{E_{opt}}{20}} \tag{12}$$

The values of the refractive index are tabulated in Table 7. The refractive index of the glass samples decreases with increasing KCl concentration. This decrease in refractive index indicates a decrease in the density of the glass samples. When selecting materials for optical systems that require specific optical properties, it is critical to consider the relationship between composition, density, and refractive index (Hussein et al. 2022; Edukondalu et al. 2017). The glasses' polarizability changes as a result of this decrease in refractive index.

The molar refractive index (R_m) can be computed using the Lorentz-Lorenz formula which is derived from the molar volume (V_m) and refractive index (N) values (Priya et al. 2021).

$$R_m=V_m\left[1-\sqrt{\frac{E_{opt}}{20}}\right] \tag{13}$$

Based on the energy band gap, refractive index, and other properties of oxides, Eqs. (14, 15, 16), are used to calculate the metallization criteria (M), molar refractive index (R_m) and molar polarizability (α_m) (Kundu et al. 2014).

$$M=1-\frac{R_m}{V_m} \tag{14}$$

$$R_m=\left(\frac{n_0^2-1}{n_0^2+2}\right)\left(\frac{M_m}{d}\right) \tag{15}$$

$$\alpha_m=\left(\frac{3}{4\pi N}\right)R_m \tag{16}$$

This correlation implies that variations in the sample's polarizability have an impact on their refractive index and molar refraction. Comprehending these correlations is essential for forecasting and analyzing the optical characteristics of the glass samples. Equation (16) transformed into relation $R_m=2.52\alpha_m$ (α_m in $Å^3$), a simple relation connecting the molar refractive index to the molar polarizability (Jeong et al. 2006).The molar polarizability and refractive index are listed in Table 7. The results show a correlation between the decrease in polarizability and with decrease in refractive index and molar refraction values. Glasses with good non-linear optical characteristics have metallization criteria values that typically vary between 0.30 and 0.45. The metallization criterion of the synthesized glasses samples has values in the range of 0.373–0.407 (Table 7). This suggests that the synthesized glass samples are within this range and they are potential candidates to be non-linear optical materials. The range of metallization parameters indicates that these glasses find use in high-power laser beam-splitting control, optical computers, memory devices, and nonlinear spectroscopy, among other areas of optics and photonics (Kundu et al. 2013).

3.5 Dielectric constant and loss

The dielectric constant and loss factor are obtained using the relationships mentioned below (Poria et al. 2024; Vijayalakshmi et al. 2017):

$$\varepsilon^*(\omega) = \varepsilon'(\omega) - j\varepsilon''(\omega) = \frac{1}{j\omega C_\circ (z' + jz'')} \tag{17}$$

$$\varepsilon' = \frac{Z''}{\omega C_\circ \left(Z'^2 + Z''^2\right)} \tag{18}$$

$$\varepsilon'' = \frac{Z'}{\omega C_\circ \left(Z'^2 + Z''^2\right)} \tag{19}$$

The dielectric loss tangent is computed with the help of:

$$tan\delta = \frac{z'}{z''} = \frac{\varepsilon''}{\varepsilon'} \tag{20}$$

where dielectric permittivity complex (ε^*), the real portion & imaginary component of the complex dielectric permittivity ($\varepsilon\prime$)&$\left(\varepsilon''\right)$, ω is angular frequency and $C_\circ$ is the capacitance.

These characteristics appear to be dependent on temperature and dopant quantity, as evidenced by the observed increases in the dielectric constant (ε ′) and loss factor (tan δ) with these variables at any frequency. Temperature and dopant concentration can change charge carrier mobility, polarization mechanisms, and dipole relaxation processes, which in turn can affect dielectric characteristics. This behavior is prevalent in dielectric materials. Figures 19 and 20 [(a and c) and (b and d)] in particular show these fluctuations for glass samples having 5, 10, 15, and 20 mol% KCl spanning a temperature range of 453–553 K, with a frequency ranging from 10^{-1} to 10^6 Hz. Temperature causes the dielectric constant to rise and frequency to decrease. Oxide glasses are known to exhibit this effect. The enhanced polarization effects caused by increased molecular motion within the glass structure are probably the cause of the dielectric constant's rise with temperature (Bahgat and Abou-Zeid 2001; Ahamad and Varma 2006). Interfacial polarization, on the other hand, is responsible for the intriguing drop in dielectric constant with frequency. When charges accumulate at interfaces, such as those between electrodes and the glass specimen, interfacial polarization happens. Higher values of the dielectric constant and loss factor result from the amount of time that charge has to build up and produce polarization effects at lower frequencies. Reduced time for charge buildup at higher frequencies leads to a decrease in interfacial polarization, which in turn causes a decrease in the dielectric constant and loss factor. This characteristic is seen in a variety of glass samples and is common for oxide glasses (Abdel-hameed et al. 2019; Sekhar et al. 2020; Kut et al. 2022).

In general, a sample's rising dielectric constant temperature is connected with a decrease in binding energies. There are two primary effects of rising temperatures on dipolar polarization:

1. *Diminished Intermolecular Interactions* This may intensify vibrations related to orientation. The material's ability to polarize can be enhanced when the bonds weaken because molecules may be more able to rotate or reorient in response to an electric field.

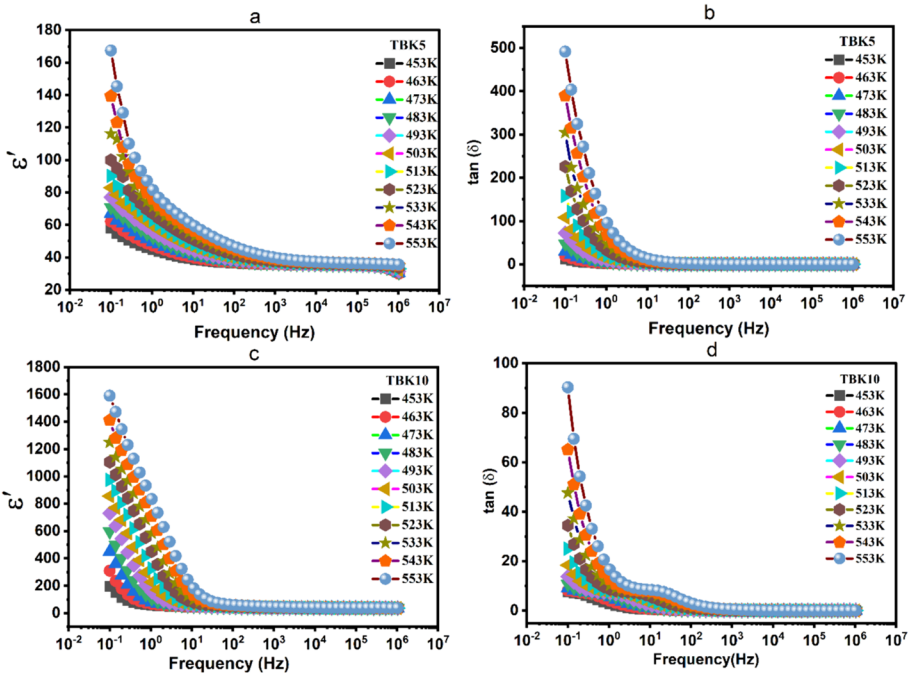

Fig. 19 Dielectric constant ε′ (a and c) and dielectric loss tan (*δ*) (b and d) variation with frequency (Hz) for glass sample $60TeO_2$-$(25-x)Bi_2O_3$-$15B_2O_3$-xKCl (x = 5, 10) at various temperatures

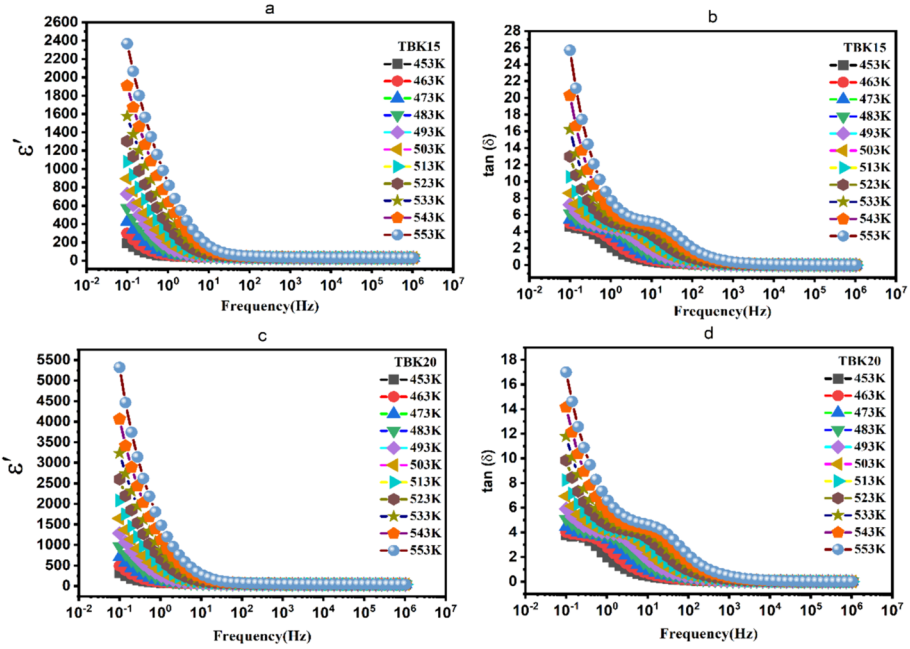

Fig. 20 Dielectric constant ε′ (a and c) and dielectric loss tan (*δ*) (b and d) variation with frequency (Hz) for glass sample $60TeO_2$-$(25-x)Bi_2O_3$-$15B_2O_3$-xKCl (x = 15, 20) at various temperatures

2. *Increase in Thermal Motion* Molecules move more thermally at higher temperatures, which might cause orientation vibrations to be disturbed. This disruption may make it more difficult for the material to polarize efficiently.

It is found that in oxide glasses, the dielectric constant tends to rise at lower frequencies and with increasing temperature. It's not always the case that this behavior indicates spontaneous polarization. There is a positive correlation between temperature and dielectric constant in some materials, such as certain types of glasses (Japari et al. 2020; Yusub et al. 2016). Ionic and electrical components contribute very little to total polarizability at low temperatures. However, the contribution from these sources starts to increase as the temperature rises. The dynamic character of the dielectric behavior demonstrates how temperature and frequency change the dielectric constant and polarizability, which in effect changes the material's validity for different applications. Photonic and electro-optic fields may see increased use of materials with low dielectric constants and loss factors at higher frequencies. These materials are especially well-suited for uses where nonlinear optical characteristics are required (Jlassi et al. 2017; Salem et al. 2018).

4 Conclusions

The quaternary glass system 60 TeO_2-(25−x) Bi_2O_3-15B_2O_3-xKCl glass series (x = 0, 5, 10, 15, and 20%) synthesized by the melt quenching technique. The amorphous nature of the synthesized glass samples has been confirmed by X-ray diffraction (XRD) and scanning electron microscopy (SEM) imaging. Using an EDX spectrum, the chemical composition of glass samples was studied. The observed decrease in density and molar volume is due to the replacement of the heavy Bi_2O_3 atoms with the lighter KCl atoms. Oxygen packing density (OPD) decreases with increasing KCl content indicating the formation of non-bridging oxygen atoms in the glass samples. DSC thermographs revealed that on the addition of KCl, glass transition temperature decreases, which is consistent with a decrease in OPD values. The FTIR and Raman investigations showed that the addition of the modifier dopant KCl causes the TeO_4 structural units to convert to TeO_3 units and BO_4 trigonal units to change into BO_3 tetragonal units. This conversion indicates the formation of non-bridging oxygen atoms in the glass network. All glasses' optical energy bandgaps (E_{opt}) were calculated using Tauc's absorption spectrum fitting techniques. The optical band gap energies increase while the Urbach energy decreases with an increase in KCl concentration in the glass samples. The computed metallization criterion value of the glass samples indicates that they are suitable for use in non-optical applications. The dielectric properties of these glasses were evaluated at various temperatures and compositions. The loss factor shows a peak at low frequency as the temperature is increased, indicating non -debye-type relaxation behavior. The glasses exhibit prospective applications in optical fibers, optoelectronics, non-linear optical technology, design laser devices, IR technologies, thermal image guides, telecommunications, and non-linear optical technology.

Acknowledgements Author Koma Poria is thankful to Maharshi Dayanand University, Rohtak for providing a University Research Scholarship ((URS. Latter No- R&S/R-15/21/URS/3949-51)) fellowship and the Department of Physics, Guru Jambheshwar University of Science and Technology Hisar, for Dielectric measurements.

Author contributions Komal Poria: Conceptualization, methodology, data curation, and writing of the original draft; Dr. Rajesh Parmar: Supervision, methodology, writing, reviewing, and editing; Dr. Sunil

Dhankhar: Writing, review, and editing; Dr. R.S. Kundu: Provide resources. All authors read and approved the final manuscript.

Funding This work was funded through the University Research Scholarship (URS. Latter No- R&S/R-15/21/URS/3949–51) fellowship. Author Komal Poria has received research support from Maharshi Dayanand University, Rohtak.

Data and materials availability Data and materials will be available on request.

Declarations

Competing interests The authors have no relevant financial or non-financial interests to disclose. The authors declare that they have no known competing financial interests or personal relationships that could have appeared to influence the work reported in this paper.

Ethical approval I have to state under my ethical responsibility that neither the manuscript nor any parts of its content are currently under consideration or published in another journal.

Consent to participate We the undersigned declare that this manuscript is original, has not been published before, and is not currently being considered for publication elsewhere. We confirm that the manuscript has been read and approved by all named authors and that there are no other persons who satisfied the criteria for authorship but are not listed. We further confirm that all have approved the order of authors listed in the manuscript.

Concept of publications We confirm that all named authors have read and approved the manuscript. We understand that the Corresponding Author is the sole contact for the Editorial process. He is responsible for communicating with the other authors about progress, submissions of revisions, and final approval of proofs.

References

Abdelghany, A.M., El-Batal, H.A., EzzEl-Din, F.M., ElAlialy, N., Okasha, A., Atta, D., Ismail, A.M., Abdelbaky, M., Aboelwafa, M.A., Awad, W.: Structural and gamma-ray attenuation of mixed former lead-free borophosphate glasses. Radiat. Phys. Chem. **214**, 111276 (2024). https://doi.org/10.1016/j.radphyschem.2023.111276

Abdel-hameed, S.A.M., Fathi, A.M., Eltohamy, M.: Structure, optical and electrical behaviour of x($2Bi_2O_3$. MnO). (10–x)B_2O_3 glasses. J. Non Cryst. Solid. **510**, 71–80 (2019). https://doi.org/10.1016/j.jnoncrysol.2019.01.010

Ahamad, M.N., Varma, K.B.R.: Crystallisation dielectric and optical characteristics of TeO_2–K_2O–Li_2O–Nb_2O_5 glasses. Phys. Chem. Glasses Eur. J. Glass Sci. Technol. B **47**, 659–664 (2006)

Ahlawat, J., Pawaria, S., Bala, M., Dahiya, S., Ohlan, A., Punia, R., Maan, A.S.: Study of thermal and physical properties of sodium modified zinc borate glasses. Mater. Today Proc. **79**, 118–121 (2023). https://doi.org/10.1016/j.matpr.2022.09.523

Akagi, R., Handa, K., Ohtori, N., Hannon, A.C., Tatsumisago, M., Umesaki, N.: High-temperature structure of K_2O–TeO_2 glasses. J. Non Cryst. Solid. **256–257**, 111–118 (1999). https://doi.org/10.1016/S0022-3093(99)00392-0

Al-Ghamdi, H., Almuqrin, A.H., Sayyed, M.I., Kumar, A.: The physical, structural and the gamma ray shielding effectiveness of the novel Li_2O-K_2O–B_2O_3–TeO_2 glasses. Result. Phys. **29**, 104726 (2021). https://doi.org/10.1016/j.rinp.2021.104726

Aloraini, D.A., Kumar, A., Almuqrin, A.H., Sayyed, M.I.: B_2O_3-TeO_2-K_2O-Li_2O glasses: optical and gamma ray shielding characterization. Optik (stuttg). **247**, 167847 (2021). https://doi.org/10.1016/j.ijleo.2021.167847

Alshamari, A., Mhareb, M.H.A., Alonizan, N., Sayyed, M.I., Dwaikat, N., Alrammah, I., Hamad, MKh., Drmosh, Q.A.: Gamma-ray-induced changes in the radiation shielding structural, mechanical, and optical properties of borate, tellurite, and borotellurite glass systems modified with barium and bismuth oxide. Optik (stuttg). **281**, 170829 (2023). https://doi.org/10.1016/j.ijleo.2023.170829

Annapurna, K., Dwivedi, R.N., Buddhudu, S.: Emission properties of Eu^{3+}: $ZnCl_2$–$BaCl_2$–KCl glass. Mater. Lett. **53**, 359–363 (2002). https://doi.org/10.1016/S0167-577X(01)00507-9

Bahgat, A.A., Abou-Zeid, Y.M.: Mixed alkali effect in the K_2O–Na_2O–TeO_2 glass system. Phys. Chem. Glas. **42**, 361–370 (2001)

Berwal, N., Kundu, R.S., Nanda, K., Punia, R., Kishore, N.: Physical, structural and optical characterizations of borate modified bismuth-silicate-tellurite glasses. J. Mol. Struct. **1097**, 37–44 (2015). https://doi.org/10.1016/j.molstruc.2015.05.011

Berwal, N., Dhankhar, S., Sharma, P., Kundu, R.S., Punia, R., Kishore, N.: Physical, structural and optical characterization of silicate modified bismuth-borate-tellurite glasses. J. Mol. Struct. **1127**, 636–644 (2017). https://doi.org/10.1016/j.molstruc.2016.08.033

Dhankhar, S., Kundu, R.S., Punia, R., Sunita, R.P., Sanjay, N.K.: Structural characterization of $ZnCl_2$ modified tellurite based glasses. AIP Conf. Proc. 1728, 020340 (2016). https://doi.org/10.1063/1.4946391

Dimitrov, V., Komatsu, T.: An Interpretation of optical properties of oxides and oxide glasses in terms of the electronic ion polarizability and average single bond strength. J. Univ. Chem. Technol. Metall. **45**, 219–250 (2010). https://doi.org/10.1016/j.jnoncrysol.2009.11.014

Edukondalu, A., Sripathi, T., Ahmmad, S.K., Rahman, S., Sivakumar, K.: Optical properties of K_2O–Li_2O–WO_3–B_2O_3 glasses: evidence of mixed alkali effect. J. Electron. Mater. **46**, 808–816 (2017). https://doi.org/10.1007/s11664-016-4949-8

Edukondalu, A., Rahman, S., Kumar, K.S.: Physical and optical properties of K_2O–TeO_2–WO_3–B_2O_3 glasses. AIP Conf. Proc. 2104, 0200006 (2019). https://doi.org/10.1063/1.5100374

Elkhoshkhany, N., El-Mallawany, R.: Optical and kinetics parameters of lithium boro-tellurite glasses. Ceram. Int. **41**, 3561–3567 (2015). https://doi.org/10.1016/j.ceramint.2014.10.182

El-Mallawany, R.A.H., El-Mallawany: Tellurite Glasses Handbook: Physical Properties and Data. CRC Press, Boca Raton (2001). https://doi.org/10.1201/9781420042085

Ersundu, M.Ç., Ersundu, A.E., Sayyed, M.I., Lakshminarayana, G., Aydin, S.: Evaluation of physical, structural properties and shielding parameters for K_2O–WO_3–TeO_2 glasses for gamma ray shielding applications. J. Alloy. Compd. **714**, 278–286 (2017). https://doi.org/10.1016/j.jallcom.2017.04.223

Farahmandjou, M., Salehizadeh, S.A.: The optical band gap and the tailing states determination in glasses of TeO_2–V_2O_5–K_2O system. Glas. Phys. Chem. **39**, 473–479 (2013). https://doi.org/10.1134/S1087659613050052

Gupta, N., Kaur, A., Khanna, A., Gonzàlez, F., Pesquera, C., Iordanova, R., Chen, B.: Structure-property correlations in TiO_2–Bi_2O_3–B_2O_3–TeO_2 glasses. J. Non Cryst. Solid. **470**, 168–177 (2017). https://doi.org/10.1016/j.jnoncrysol.2017.05.021

Haizheng, T., Xiujian, Z., Chengbin, J.: Raman spectroscopic study on the microstructure of GeS_2–Ga_2S_3–KCl glasses. J. Mol. Struct. **697**, 23–27 (2004). https://doi.org/10.1016/j.molstruc.2003.12.039

Haizheng, T., Xiujian, Z., Wei, T., Shun, M.: Micro-structural study of the GeS_2–In_2S_3–KCl glassy system by Raman scattering. Spectrochim. Acta-Part Mol. Biomol. Spectrosc. **64**, 1039–1045 (2006). https://doi.org/10.1016/j.saa.2005.09.013

Hussein, K.I., Al-Syadi, A.M., Alqahtani, M.S., Elkhoshkhany, N., Algarni, H., Reben, M., Yousef, E.S.: Thermal Stability, Optical Properties, and Gamma Shielding Properties of Tellurite Glass Modified with Potassium Chloride. Materials (basel). **15**, 1–17 (2022). https://doi.org/10.3390/ma15072403

Ibrahim, S., Abo-Mosallam, H.A., Mahdy, E.A., Turky, G.M.: Impact of high NiO content on the structural, optical, and dielectric properties of calcium lithium silicate glasses. J. Mater. Sci. Mater. Electron. **33**, 10596–10610 (2022). https://doi.org/10.1007/s10854-022-08045-8

Japari, S.J., Yahya, A.K., Hisam, R.: Effects of mixed-alkali oxides on AC conductivity and dielectric properties of xNa_2O–$(20–x)K_2O$–$30V_2O_5$–$50TeO_2$ glasses. Result. Phys. **16**, 102905 (2020). https://doi.org/10.1016/j.rinp.2019.102905

Jeong, E.D., Ha, M.G., Pak, H.K., Ryu, B.K., Borse, P.H., Lee, J.S., Komatsu, T., Kim, H.J., Kim, H.G.: Thermal stabilities, physical and optical properties of K_2O–Na_2O–Nb_2O_5–TeO_2 glasses. J. Ind. Eng. Chem. **12**, 926–931 (2006)

Jlassi, I., Sdiri, N., Elhouichet, H.: Electrical conductivity and dielectric properties of MgO doped lithium phosphate glasses. J. Non Cryst. Solid. **466–467**, 45–51 (2017). https://doi.org/10.1016/j.jnoncrysol.2017.03.042

Karthika, S., Sundari, S.S., Marimuthu, K., Meena, P.: Enhancement of electrical and radiation shielding properties of vanadium doped lithium telluro-borate (LTB) glasses. Chem. Phys. Impact. **8**, 100430 (2023). https://doi.org/10.1016/j.chphi.2023.100430

Kashif, I., Ratep, A., Adel, G.: Polarizability, optical basicity and optical properties of SiO_2–B_2O_3–Bi_2O_3–TeO_2 glass system. Appl. Phys. **124**, 1–9 (2018). https://doi.org/10.1007/s00339-018-1904-y

Kaushik, H.K., Kaur, A., Garg, V., Km Abida, S., Kumar, K., Singh, S.P., Singh, S.K.: Effect of CuO on physical, structural and optical properties of lithium borosilicate glasses. Mater. Today Commun. **35**, 106208 (2023). https://doi.org/10.1016/j.mtcomm.2023.106208

Kundu, R.S., Dhankhar, S., Punia, R., Sharma, S., Kishore, N.: $ZnCl_2$ modified physical and optical properties of barium tellurite glasses. Trans. Indian Ceram. Soc. **72**, 206–2010 (2013). https://doi.org/10.1080/0371750X.2013.851883

Kundu, R.S., Dhankhar, S., Punia, R., Nanda, K., Kishore, N.: Bismuth modified physical, structural and optical properties of mid-IR transparent zinc boro-tellurite glasses. J. Alloy. Compd. **587**, 66–73 (2014). https://doi.org/10.1016/j.jallcom.2013.10.141

Kundu, R.S., Dult, M., Punia, R., Parmar, R., Kishore, N.: Titanium induced structural modifications in bismuth silicate glasses. J. Mol. Struct. **1063**, 77–82 (2014)

Kundu, R.S., Dhankhar, S., Punia, R., Dult, M., Kishore, N.: Thermal and structural properties of zinc modified tellurite based glasses. AIP Conf. Proc. 1731, 070039 (2016).

Kut, T.V.N.K., Marijan, S., Pisk, J., Sekhar, A.V., Reddy, A.S.S., Venkatramaiah, N., Raju, G.N., Pavić, L., Veeraiah, N.: Impact of silver ions on dielectric properties and conductivity of lithium silicate glass system mixed with red lead. J. Non Cryst. Solid. **588**, 121641 (2022). https://doi.org/10.1016/j.jnoncrysol.2022.121641

Lee, K.H., Kim, T.H., Kim, Y.S., Jung, Y.J., Na, Y.H., Ryu, B.K.: Structural modification of alkali tellurite binary glass system and its characterization. Korean J. Mater. Res. **18**, 235–240 (2008). https://doi.org/10.3740/MRSK.2008.18.5.235

Marzuki, A., Sasmi, T., Fausta, D.E., Harjana, H., Suryanti, V., Kabalci, I.: The effect of Bi_2O_3/PbO substitution on physical, optical, structural, and gamma shielding properties of boro-tellurite glasses. Radiat. Phys. Chem. **205**, 110722 (2023). https://doi.org/10.1016/j.radphyschem.2022.110722

McGlashan, A., Nelson, P.N., Prasad, P.S., Iezid, M., Goumeidane, F., Rajaramakrishna, R., Rao, P.V.: Physical, thermal, optical, shielding and elastic properties of Bi_2O_3–B_2O_3–TeO_2 glass system doped with Fe_2O_3. Radiat. Phys. Chem. **217**, 111444 (2024). https://doi.org/10.1016/j.radphyschem.2023.111444

Pandarinath, M.A., Upender, G., Rao, K.N., Suresh Babu, D.: Thermal, optical and spectroscopic studies of boro-tellurite glass system containing ZnO. J. Non Cryst. Solid. **433**, 60–67 (2016). https://doi.org/10.1016/j.jnoncrysol.2015.11.028

Poria, K., Dhankhar, S., Rajesh Parmar, R.S., Kundu, R.B.: Effect of $ZnCl_2$ on structural and optical features of TeO_2–B_2O_3–Bi_2O_3–$ZnCl_2$ glasses. Solid State Sci. **142**, 107239 (2023). https://doi.org/10.1016/j.solidstatesciences.2023.107239

Poria, K., Parmar, R., Dhankhar, S., Kundu, R.S.: Electrical conductivity and hopping conduction mechanism by VRH model in halide modified tellurite glasses. Solid State Sci. **148**, 107442 (2024). https://doi.org/10.1016/j.solidstatesciences.2024.107442

Priya, G.K., Yusub, S., Babu, A.R., Ram, N.S., Krishna, K.R., Aruna, V.: The eminence of copper ions on optical, electrical properties and morphology of B_2O_3–Bi_2O_3–Al_2O_3–MgO glasses. J. Non Cryst. Solid. **568**, 120844 (2021)

Rammah, Y.S., Ali, A.A., El-Mallawany, R., Abdelghany, A.M.: Optical properties of bismuth borotellurite glasses doped with $NdCl_3$. J. Mol. Struct. **1175**, 504–511 (2019). https://doi.org/10.1016/j.molstruc.2018.07.071

Rani, S., Ahlawat, N., Parmar, R., Dhankhar, S., Kundu, R.S.: Role of lithium ions on the physical, structural and optical properties of zinc boro tellurite glasses. Indian J. Phys. **92**, 901–909 (2018a). https://doi.org/10.1007/s12648-018-1164-x

Rani, A., Parmar, R., Kundu, R.S.: Structural, physical, thermaz, and optical analysis of lead modified bismo-borovanadate glassy system: V_2O_5–B_2O_3–Bi_2O_3–PbO. J. Inorg. Organomet. Polym. Mater. **34**, 1589–1608 (2023). https://doi.org/10.1007/s10904-023-02896-2

Rani, S., Kundu, R.S., Ahlawat, N., Rani, S., Sangwan, K.M., Ahlawat, N.: Effect of lithium on thermal and structural properties of zinc vanadate tellurite glass. In AIP Conference Proceedings. 1942, 07002610 (2018b). 1063/1.5028824

Saddeeka, Y.B., Alya, K.A., Shaabanc, K.S., Alid, A.M., Alqhtanid, M.M., Alshehrid, A.M., Sayedd, M.A., Wahaba, E.A.A.: Physical properties of B_2O_3–TeO_2–Bi_2O_3 glass system. J. Non Cryst. Solid. **498**, 82–88 (2018). https://doi.org/10.1016/j.jnoncrysol.2018.06.002

Salem, S.M., Mansour, S.F., Bashter, I.I., MSadeq, S., Mostafa, A.G.: Effect of mixed heavy metal cations on the A.C. conductivity and dielectric properties of some boro-silicate glasses. Ceram. Int. **44**, 14363–14369 (2018). https://doi.org/10.1016/j.ceramint.2018.05.045

Samee, M.A., Edukondalu, A., Ahmmad, S.K., Taqiullah, SMd., Rahman, S.: Mixed-alkali effect in Li_2O–Na_2O–K_2O–B_2O_3 glasses: infrared and optical absorption studies. J. Electr. Mater. **42**, 2516–2524 (2013). https://doi.org/10.1007/s11664-013-2605-0

Saritha, D., Markandeya, Y., Salagram, M., Vithal, M., Singh, A.K., Bhikshamaiah, G.: Effect of Bi_2O_3 on physical, optical and structural studies of ZnO–Bi_2O_3–B_2O_3 glasses. J. Non Cryst. Solid. **354**, 5573–5579 (2008). https://doi.org/10.1016/j.jnoncrysol.2008.09.017

Sekhar, A.V., Pavi, L., Mogu, A., Purnachand, N., Reddy, A.S.S., Raju, G.N., Veeraiah, N.: Dielectric characteristics, dipolar relaxation dynamics and ac conductivity of CuO added lithium sulpho-phosphate glass system. J. Non Cryst. Solid. **543**, 120157 (2020)

Sidkey, M.A., Gaafar, M.S.: Ultrasonic studies on network structure of ternary TeO_2–WO_3–K_2O glass system. Phys. B Condens. Matter. **348**, 46–55 (2004). https://doi.org/10.1016/j.physb.2003.11.005

Singh, L., Thakur, V., Punia, R., Kundu, R.S., Singh, A.: Structural and optical properties of barium titanate modified bismuth borate glasses. Solid State Sci. **37**, 64–71 (2014). https://doi.org/10.1016/j.solidstatesciences.2014.08.010

Takebe, H., Nishimoto, S., Kuwabara, M.: Thermal and optical properties of CuO–BaO–B_2O_3–P_2O_5 glasses. J. Non Cryst. Solid. **353**, 1354–1357 (2007). https://doi.org/10.1016/j.jnoncrysol.2006.09.044

Thakur, V., Singh, A., Punia, R., Dahiya, S., Singh, L.: Structural properties and electrical transport characteristics of modified lithium borate glass ceramics. J. Alloy. Compd. **696**, 529–537 (2016). https://doi.org/10.1016/j.jallcom.2016.11.230

Thanigaiselvan, R., Raja, T.S.R., Karthik, R.: Investigations on Eco friendly insulating fluids from rapeseed and pongamia pinnata oils for power transformer applications. J. Electr. Eng. Technol. **10**, 2348–2355 (2015). https://doi.org/10.5370/JEET.2015.10.6.2348

Tolga Gorgulu, A., Cankaya, H., Kurt, A., Speghini, A., Bettinelli, M., Sennaroglu, A.: Spectroscopic characterization of Tm^{3+}:TeO_2–K_2O–Nb_2O_5 glasses for 2-μm lasing applications. J. Lumin. **132**, 110–113 (2012). https://doi.org/10.1016/j.jlumin.2011.07.004

Vijayalakshmi, L., Kumar, K.N., Kumar, G.B., Hwang, P.: Structural, dielectric and photoluminescence properties of Nd^{3+} doped Li_2O–LiF–B_2O_3–ZnO multifunctional optical glasses for solid state laser applications. J. Non Cryst. Solid. **475**, 28–37 (2017). https://doi.org/10.1016/j.jnoncrysol.2017.08.024

Wang, P., Wang, C., Li, W., Lu, M., Peng, B.: Effects of Al_2O_3 on the thermal stability, glass configuration of Yb^{3+}–doped TeO_2–K_2O–ZnO–Al_2O_3 based tellurite laser glasses. J. Non Cryst. Solid. **359**, 5–8 (2013). https://doi.org/10.1016/j.jnoncrysol.2012.09.031

Yusub, S., Rao, P.S., Rao, D.K.: Ionic conductivity, dielectric and optical properties of lithium lead borophosphate glasses combined with manganese ions. J. Alloy. Compd. **663**, 708–717 (2016). https://doi.org/10.1016/j.jallcom.2015.12.147